Use of functionally graded material layers in a two-layered pressure vessel

E. Carrera*, M. Soave
Department of Aeronautics and Space Engineering
Politecnico di Torino, Italy

PAPER REF: PVT -09-1198

VERSION ACCEPTED ON NOV 23rd 2010.

Abstract

This work explores the possibilities of using functionally graded material layers to reduce normal and shear stress gradients due to internal pressure and thermal loadings at the interface of a two layered wall pressure vessel. The two walls are made of an internal thin metallic layer (Titanium, used as a liner to avoid a chemical/physical reaction between the gas and the external layer) and an external thick layer (carbon fiber used as a structural restraint). Two main geometrical elements are investigated: a cylindrical shell and a spherical panel. The Shell analysis has been made by referring to mixed layer-wise theories which lead to a three-dimensional description of the stress/strain fields in the thickness shell direction; results related to first order shear deformation theory are given for comparison purposes. It has been concluded that it is convenient to use FGM layers to reduce shear and normal stress gradients at the interfaces. Furthermore, the FGM layers lead to benefits as far as buckling load is concerned; lower values of in-plane shear and longitudinal compressive stress are in fact obtained with respect to a pure two-layered wall.

*Author for correspondence: Erasmo Carrera, Professor. Department of Aeronautics and Space Engineering, Politecnico di Torino, Corso Duca degli Abruzzi, 24, 10129 Torino, ITALY, tel: +39.011.090.6836, fax: +39.011.564.6899. e.mail: erasmo.carrera@polito.it.

1 Introduction

Pressure vessels are defined as containers with a pressure differential between the inside and outside; the inside pressure is usually higher than the outside one, except in some cases such as in submarine applications. Tanks, vessels and pipelines that carry, store and receive fluids are called pressure vessels. High pressure is often combined with high temperature, flammable fluids or radioactive materials; because of these hazards, it is mandatory that the design be such that no leakage can occur. In addition, these vessels have to be designed carefully to cope with the operating temperature and pressure. Plant safety and integrity are of fundamental concern in pressure vessel design and these, of course, depend on the adequacy of the design code.
The size and geometric form of pressure vessels vary greatly from the large cylindrical vessels used for high pressure gas storage to the small sized ones, used as hydraulics units for aircraft, see the recent book by Chattopadadhyay [1]. Pressure vessels are usually spherical or cylindrical with dome ends. Safety is the main concern in many applications, such as in nuclear power plants. The possible risk of a given mode of failure and its consequences are balanced against the effort required for its prevention; the resulting design should achieve an adequate standard of safety at a minimum cost. The design factor used in the ASME Pressure Vessel Code is intended to account for unknown factors associated with the design and construction of the equipment; interesting discussion on the use of ASME pressure vessels code for various applications is given in [1].

In recent years, many works on pressure vessels have been published, due to the possibility of their use in engineering applications. An important contribution to the study of pressure vessels for space applications was has been made by Bushnell. In the book [2], in fact, the theoretical study is supported by BOSOR computer application (acronym for Buckling of shells of revolution) that allowed, already back in those years, a study to be made of computer-pressure vessels through different types of analysis: nonlinear static analysis, the study of buckling and vibration. More recently, Zhang et al. in [3] and in [4] have studied spherical tanks which were built using the integral hydro-bulge forming technology in China in 1992. In these works, a three-dimensional elasto-plastic finite element method is used to analyse the hydro-bulging process of the tank: the deformation process and the deformation features have been revealed, and the stress and strain distributions have been analyzed. Baum in [5] shows that, when there is a circumferential fracture of a cylindrical pressure vessel containing high-pressure gas, the internal pressure falls as gas escapes through the developing breach. If the break is adjacent to the end-cap, the end-cap will be accelerated by the escaping gas. Khan and Uddin in [6] have studied the instability under pressure of conical end caps with spherical tips when used as end closures to pressure vessels. The results show that the critical pressure for the end closure decreases with increasing apex angle. A numerical analysis study using the finite element method has been carried out by Tafreshi in [7] to investigate the design sensitivity of thin torispherical end pressure vessels. The buckling pressure and stresses in a series of torispherical ends have been evaluated to show the effect of variations in the shape parameters in these ends. Mackerle in [8], [9] and [10] gives a review on finite element methods(FEMs) applied for the analysis of pressure vessel structures, components and piping, from the theoretical and practical points of view. Another topic of particular interest is the welding procedure regarding pressure vessels. Li and Gobbi in [11] describe potential applications of high-power CO, and Nd lasers to create lightweight structures in the automotive, aeronautic and aerospace industries. The purposes of the research were to examine the possibility of assembling lightweight structures with minimal deformation, reducing the total weight by combining current laser-welding techniques with particular structural designs, and improving properties and performance. Teng and Lin in [12] have presented an innovative technique for the fabrication of small models of large steel cylindrical shells constructed with many welded panels. The experimental set-ups used to implement this technique in the laboratory are also described.

Among the most recent applications, pressure vessels with very high pressure for space applications

are of interest. These high pressure tanks can be used to store propellent for satellites and space vehicles. Applications could also consider hydrogen storage in the automotive industry in the framework of green car projects. Considerations on weight, see also Sec. 4.2, clearly show the advantage of using carbon-fibers. A carbon fiber wall is build by employing a filament winding technique. This technique is based on using a liner on which fibers are wrapped. These fibers are made of durable material which forms the main structure of the vessel. Jones et al. in [13] have described a filament winding process that results in a constant thickness lay-out of composite over the end closures of a dome-ended cylindrical vessel. An experimental design investigation of manufacturing and design variables that affect composite vessel quality, strength, and stiffness has been conducted by Cohen in [14]. The material and processing variables were divided into five categories: (a) resin, (b) fiber, (c) fabrication process, (d) design, and (e) equipment. A statistical analysis of the data has shown that the composite vessel strength is affected by the manufacturing and design variables. Cohen et al. in [15] have offered a continuation of the previous research which included a design of an experiment investigation of manufacturing and design variables that affect composite vessel quality and strength.

Unfortunately, carbon fiber cannot be in contact with the gasses, such as helium and hydrogen, which are used in these high pressure tanks. A liner must therefore be used to avoid contact. The liner therefore has a double aim: to wrap the carbon fibers in the filament winding technique and to separate the liquified gas from the carbon. The thickness of the liner is obviously much lower than that of the main structure,in order to exploit the chemical and physical properties without burdening the overall weight of the structure. The choice of material for the liner is mainly influenced by the type of fluid that the vessel must contain. In order to avoid corrosion problems it is important to use metals that are compatible with the gas and at the same time present weldability characteristics to satisfy the structural requirements. The discontinuity at the interfaces between the layers leads to additional complications. For instance, in the case of filament winding, the presence of an adhesive could create mechanical problems for the whole structure. The choice for the liner often falls on Titanium as because of its high resistance to corrosion.

This paper aims to contribute to the design and analysis of composite made pressure vessels with metallic thin layers liner. In order to reduce/remove discontinuities at the interface between the Titanium and Carbon fiber, the present work explores the possibilities of using functionally graded material (FGM) layers as interface between liner and composite made structural restraint. FGM consists of material, mostly panels and shells, in which the mechanical/thermal properties varies along the thickness directions. In most case FGM panels are made by using a large number of thin layer with almost continuous variation of mechanical properties in the thickness direction [16], [17]. Such a feature permits to reduce mechanical discontinuity between layers of different materials (as it is in the sandwich structures and in the pressure vessels which are of interest for this work) and related interlaminar stress fields can be strongly modified. Applications of FGM are also considered to build the walls of engine chambers or rocket nozzles which require high-temperature resistant materials (see [18]). A recent review on FGM, including applications and modeling is given in the review article [19]. FGM are in this work used between Titanium and carbon fibers. A continuous variation of the Young Modulus is assigned from that of Titanium to that of the carbon fibers. For sake of simplicity the attention has been restricted only to representative structural components. More complex analysis could be considered by future work. Two main pressure vessel components are considered: a cylindrical shell and a spherical cap. A layer wise mixed shell theory has been employed to handle the continuous variation of mechanical properties in the thickness direction in appropriate manner. Results related to the shear deformation theories that are usually provided by the FE-shell commercial codes are considered for comparison purposes. Mechanical and thermal loadings are considered. Stress and displacements are compared in most of the conducted analysis. The results are restricted to those cases for which Navier type closed form solutions are available. It holds only for harmonic distribution of loading which could be combined to give constant pressure. That would not lead to changes in the paper conclusions.

2 Pressure vessels geometry

Cylindrical vessels with spherical end caps are considered in this works. Only two significant geometrical parts of the full vessels are treated. These two elements refer to a cylindrical shell (ring) and to a spherical panel taken from the caps, see Figure 1. Authors believe that the conclusion reached in the present work are not affected by shell geometries. On the other hand, closed form solutions can be easily found only for the above mentioned shell elements.
Shells radii are denoted by R_α and R_β along the two in-plane directions α and β respectively; curvilinear reference system (α, β, z) for shells is indicated in Figure 2 where the ring geometry is given. For the cylindrical shell α coincides with the circumferential coordinate and the external and internal radius of cylinder R_e and R_i are defined; β is the longitudinal direction along with the length L is defined. Wall lay-up geometries is given in Figure 3; the flat case related to the longitudinal direction of the cylinder has been drawn, cylindrical and shell geometries should be considered in the other cases. The two cases under analysis are described: the original two-layered wall (titanium, carbon fiber) is on the left side while the wall including a functionally graded material layer is on the right side.

3 Classical and layer-wise mixed used shell theories

Shell analysis is herein conducted by employing the Carrera Unified Formulation (CUF) [20], [21], [22]. Quasi three-dimensional description of stress states in the layer is acquired upon application of a layer-wise mixed shell theories with quartic-ordered of expansion for both displacements and transverse stress variables in the shell thickness directions. The most known and applied First order Shear Deformation shell theories FSDT, is also considered for comparison purposes. Details of CUF can be found in the above mentioned first authors articles, further application to FGM structures have been more recently given in [24], [25]. Few details of the two referred shell theories are given below.
Transverse shear deformations theory, FSDT, introduced according to Reissner and Mindlin's kinematic assumptions leads to the following displacement fields:

$$\begin{array}{l} u_\tau(\alpha,\beta,z) = u_{0\tau}(\alpha,\beta) + z \;\; u_{1\tau}(\alpha,\beta) \quad \text{with} \quad \tau = \alpha,\beta,z \\ u_z(\alpha,\beta,z) = u_{0z}(\alpha,\beta). \end{array} \tag{1}$$

where u are the displacements along α, β and z coordinates, u_0 denotes the displacements value in correspondence to the reference surface Ω and u_1 is the first derivative of u_0 along the in-plane coordinates α and β. Transverse shear stresses computed by FSDT shows "a priori" constant piece-wise distribution.
Layerwise multilayered shells theories refer to kinematics assumptions which are independent in each layer k. According to [23] these approaches are herein stated as Layer-Wise (LW) theories. The Taylor thickness expansion, adopted for FSDT case, is not convenient for LW description. Displacements interlaminar continuity can be imposed more conveniently by employing interface values as unknown variables. This description can be applied to displacement components $\boldsymbol{u} = (u_\alpha, u_\beta, u_z)$ and transverse shear and normal stresses $\boldsymbol{\sigma}_n = (\sigma_{\alpha z}, \sigma_{\beta z}, \sigma_{zz})$. Layer Wise description is introduced according to the following expansion:

$$(\boldsymbol{u^k}, \boldsymbol{\sigma}^k_n) = \; F_t \; (\boldsymbol{u}^k_t, \boldsymbol{\sigma}^k_{nt}) \; + \; F_b \; (\boldsymbol{u}^k_b, \boldsymbol{\sigma}^k_{nb}) \; + \; F_l \; (\boldsymbol{u}^k_l, \boldsymbol{\sigma}^k_{nl}) = \; F_\tau \; (\boldsymbol{u}^k_\tau, \boldsymbol{\sigma}^k_\tau) \tag{2}$$

where

$$\tau = t, b, l \quad with \quad l = 2, \ldots, N$$

t, b subscripts denote top and bottom values in the k-layer of displacement/stress variables, respectively; while l refer to higher order values. The thickness functions $F_\tau(\zeta_k)$ have now been defined at the k-layer

level, they are a linear combination of Legendre polynomials $P_j = P_j(\zeta_k)$ of the j^{th}-order defined in ζ_k-domain ($\zeta_k = \frac{2z_k}{h_k}$ with z_k local coordinate and h_k thickness, both referred to k^{th} layer, so $-1 \leq \zeta_k \leq 1$). The first five Legendre polynomials are:

$$P_0 = 1, \;\; P_1 = \zeta_k, \;\; P_2 = \frac{(3{\zeta_k}^2 - 1)}{2}, \;\; P_3 = \frac{5{\zeta_k}^3}{2} - \frac{3\zeta_k}{2}, \;\; P_4 = \frac{35{\zeta_k}^4}{8} - \frac{15{\zeta_k}^2}{4} + \frac{3}{8} \tag{3}$$

their combinations for the thickness functions are:

$$F_t = \frac{P_0 + P_1}{2}, \;\; F_b = \frac{P_0 - P_1}{2}, \;\; F_l = P_l - P_{l-2} \quad with \quad l = 2, \ldots, N \tag{4}$$

The chosen functions have the following interesting properties:

$$\zeta_k = 1 \quad : \; F_t = 1; \;\; F_b = 0; \;\; F_l = 0 \quad at\ top \tag{5}$$

$$\zeta_k = -1 \; : \; F_t = 0; \;\; F_b = 1; \;\; F_l = 0 \quad at\ bottom \tag{6}$$

That is interface values of the variables are considered as variable unknowns.
LW model can be conveniently used even though a plate is constituted by only one layer, via the introduction of mathematical interfaces and by using a N order of expansion in the corresponding fictitious layers. Accuracy of the solution can be increased by increasing the number of the mathematical interfaces. The case N=4 has been implemented in the present work. Additional details of governing differential equations and boundary conditions are given in the Appendix.

4 Numerical Investigation and Discussion

A numerical investigation has been conducted to explore the possible advantages of using FGM made pressure vessel walls. Cylindrical shell and spherical panels are considered and subjected to mechanical and thermal loadings. The analysis of connections between spherical caps and cylinder, even though these represent a crucial point of pressure vessels design [1], are out-of-scope of the present work which is direct to a preliminary instigation on the advantages/disadvantages of using FGM layers to build pressure vessel layered walls.

4.1 Closed-form solutions

Closed-form solutions of the governing equations (see the Appendix A) of double laminated curved shells made up of orthotropic layers are considered in this section. Details of the differential equations and Navier type solutions can be found in [29]. The shells are loaded by a harmonic distribution of the transverse pressure:

$$p_z(\alpha, \beta) = \hat{p}_z(\alpha, \beta) \sin\frac{m\pi\alpha}{a} \;\; \sin\frac{n\pi\beta}{b}, \tag{7}$$

a and b denote the shell lengths in the α and β directions, respectively (in the case of a cylindrical shell $a = 2\pi R_\alpha$ and $b = L$, see Figure 2). The displacements in each layer k are assumed of the following form:

$$\begin{aligned}
u^k_{\alpha_\tau} &= \textstyle\sum_{m,n} (\hat{U}^k_{\alpha_\tau}) \cos\frac{m\pi\alpha_k}{a_k} \;\; \sin\frac{n\pi\beta_k}{b_k} && k = 1, N_l \\
u^k_{\beta_\tau} &= \textstyle\sum_{m,n} (\hat{U}^\beta_{y_\tau}) \sin\frac{m\pi\alpha_k}{a_k} \;\; \cos\frac{n\pi\beta_k}{b_k} && \tau = t, b, l \\
u^k_{z_\tau} &= \textstyle\sum_{m,n} (\hat{U}^k_{z_\tau}) \sin\frac{m\pi\alpha_k}{a_k} \;\; \sin\frac{n\pi\beta_k}{b_k} && l = 2, N
\end{aligned} \tag{8}$$

where $\hat{U}^k_{\alpha_\tau}$, $\hat{U}^k_{\beta_\tau}$ and $\hat{U}^k_{z_\tau}$ are the amplitudes, m and n are the wave numbers and a_k and b_k are the shell dimensions which correspond to simply supported boundary conditions The maximum displacement

and stresses values are considered in the following analysis, unless other values are explicitly declared. In the case of thermal loadings, the temperature is assumed to vary linearly in the thickness direction by using a unit gradient, while the in-plane distribution is given by the following formula:

$$T(\alpha, \beta, z) = T(z) \sin \frac{m\pi\alpha}{a} \ \sin \frac{n\pi\beta}{b}, \tag{9}$$

4.2 Pressure Vessel elements loaded by internal pressure

Data of typical materials that could be used in pressure vessel construction are given in Table 1 where E is the young modulus, ρ is the density, σ_f is the allowable stress and ν is the Poisson ratio. A comparison of the performance of these materials is given for the cylindrical shell case in Table 2. Cylinders constituted by a metallic and carbon fiber wall of the same volume are considered (same thickness). The geometrical data of the shell is as follows: the internal radius R_i is fixed to 0.4 $[m]$, the length along the β direction L is 1 $[m]$, the radii are $R_\alpha = 1[m]$, $R_\beta = \infty[m]$ and the external radius R_e is a function of thickness h, which varies according to the analysis.

Table 2 compares the weight [W] of the three metallic walls with that of the carbon fiber ones. The maximum pressure $p_{Max}$is also given. The advantage using carbon fiber is very evident. Figure 4 shows the maximum pressures vs the wall thickness. The Von Mises yielding criteria σ_{Eq} has been used for comparison purposes. The advantage of using carbon fiber has been confirmed.

4.2.1 Cylindrical shell with FGM layers

Three layered walls are considered with the following geometrical data:

Ti/C Titanium liner (h=0.01[m]) and carbon fiber wall (h=0.09[m]) with $h_{tot} = 0.1[m]$

FGM Titanium liner (h=0.01[m]) FGM layer (h=0.02[m]) carbon fiber wall (h=0.07[m]) with $h_{tot} = 0.1[m]$

FGM* Titanium liner (h=0.01[m]) FGM layer (h=0.02[m]) carbon fiber wall (h=0.09[m]) with $h_{tot} = 0.12[m]$

The wall data are summarized in Table 3. The distribution of the Young modulus in the wall direction is given in Figure 5. The third case, denoted as $FGM*$, is heavier than the other two ones. It shows the possible advantages of adding additional FGM layers to the two existing walls. Table 4 shows the weight, the maximum stresses and the interlaminar shear stresses for the three analyzed configuration: $\tau_{i.l.}(1)$ is the interlaminar stress between the Titanium liner and the FG layer while $\tau_{i.l}(2)$ is the same stress between the FG layer and the main Carbon fiber structure. The advantage of using the FGM layers, with respect to maximum shear stresses, has been confirmed. The advantages of the $FGM*$ wall, with respect to the maximum equivalent stress, is also evident. Figures 6 and 7 compare the variations in displacement and stresses along the thickness for the three configurations. It should be pointed out, that the $FGM*$ case refers to a thicker wall. As a consequence the cylinder shows higher stiffness in the FGM* case and related displacements are lower than TI/C and FGM cases. The latter is the most deformable one. σ_{eq} plot shows that the FGM* wall correspond to the lowest gradient at the Titanium-Carbon interface.

The capability of FGM layers to reduce discontinuous stress fields is clearly evident; the transverse shear stress barely increases in the FGM case, due to higher shear deformations of the FGM layer with respect to Titanium.

Tables 4 and 5 provide a detailed comparison, in terms of shear and normal stress as well as in terms of maximum allowable pressure p related to a von-Mises criterion (which is dominated by normal stress values), and to a shear stress criterion which is dominated by $\tau_{i.l.}$. The lower values of $\tau_{i.l.}$ could reduce

the possibility of delamination growth. The analysis shows that the presence of FGM layers leads to an increase in the allowable pressure $\Delta p = 54.00\ MPa$, which corresponds to 2.93%, where Δp is the difference between the classical laminate and the FGM wall values. Such a relatively small percentage could become very significant in space mission design.
The following relevant conclusions can be drawn considering the in-plane stress results:

- The use of FGM layers leads to a strong reduction in the circumferential normal stress $\sigma_{\alpha\alpha}$ values.
- The strong reduction in the compressive values of the longitudinal stress $\sigma_{\beta\beta}$ and the shear stress $\sigma_{\alpha\beta}$ introduced by the FGM layers is of particular interest. That is the *FGM* layers are expected to increase the buckling resistance of the wall.In other words, the local buckling phenomena, which are one of the most relevant design requirements for two-layered made pressure vessels, are reduced by the FGM layers.

Figure 8 shows that FSDT analyses, such as those available in commercial FE codes, are ineffective in tracing the stress behavior in the thickness directions. The use of FSDT shell elements could lead to completely erroneous conclusions. Better results could be reproduced by using solid elements, which could lead to a significant increase of the computational costs.

4.3 Spherical cap loaded by internal pressure

Similar results have been derived for the spherical panels, as confirmed in Figure 9. The data are the same as those of the previous section. The FGM layer leads to continuity for transverse stress components; discontinuity is reduced for in-plane stresses with respect to the original spherical two-layered wall panel. In plane shear stresses are reduced when a FGM layer is used. As in the cylindrical case the FGM layers are expected to increase the buckling resistance of the wall in both case of longitudinal and shear stresses. To be noticed that present analysis has been limited to spherical panels that are considered as part of a spherical pressure vessel. In that case the stress fields do not change over the shell reference surface. In practical cases the spherical parts are connected to the cylindrical shell and the above assumption could result not applicable.

4.4 Cylindrical shell subjected to thermal loading

A thermal stress analysis has also been conducted. The temperature distribution in the shell thickness is not assumed linear, but is computed by solving the Fourier heat conduction equation. For the k^{th} homogeneous orthotropic layer, the differential Fourier's equation of heat conduction reads:

$$\left(\frac{K_1^k}{H_\alpha^2}\right)\frac{\partial^2 T}{\partial \alpha^2} + \left(\frac{K_2^k}{H_\beta^2}\right)\frac{\partial^2 T}{\partial \beta^2} + K_3^k\,\frac{\partial^2 T}{\partial z^2} = 0\ , \tag{10}$$

K_1^k, K_2^k and K_3^k are the thermal conductivities along the three shell directions α, β and z; they are constant in each layer in case of classical materials, but they depend by the thickness coordinate in case of FGMs. ∂ indicates the partial derivative. $H_\alpha = (1 + z^k/R_\alpha^k)$ and $H_\beta = (1 + z^k/R_\beta^k)$ are the metric coefficients. In case of plates the Eq.(10) has $H_\alpha = H_\beta = 1$ and the coefficients K_1^k, K_2^k and K_3^k depend on z because some layers k can be in FGM. In case of shell we can define three new coefficients $K_1^{*k} = \frac{K_1^k(z)}{H_\alpha^2}$, $K_2^{*k} = \frac{K_2^k(z)}{H_\beta^2}$ and $K_3^{*k} = K_3^k(z)$, which in a generic layer k depend on the thickness coordinate of the shell. K_1^{*k} and K_2^{*k} can depend by the thickness coordinate z for two reasons: possible use of FGM layers and/or presence of curvature in case of shells; K_3^{*k} can depend by z coordinate only in case of FGM layers. So:

$$K_1^{*k}\,\frac{\partial^2 T}{\partial \alpha^2} + K_2^{*k}\,\frac{\partial^2 T}{\partial \beta^2} + K_3^{*k}\,\frac{\partial^2 T}{\partial z^2} = 0\ . \tag{11}$$

That equation has been solved according to the closed form solution technique which has been extensively described the authors articles [30], [31], and [32]. For sake of concisennes the governing equations for the thermomechanical cases are omitted, these can be found in [32].
Interface discontinuities are eliminated by the FGM layer, as in the mechanical loading case. In-plane shear maximum values are reduced by reducing buckling failure, (Figure 10). This reduction appears more significant that those found in the case of mechanical loadings. That is, by grading thermal properties major advantages are obtained.

5 Conclusions

This work has shown the advantage of using an FGM layer in a two-layered pressure vessel wall with a layer-liner in Titanium and a structural restraint-layer made of Carbon fibers. FGM layers reduce interlaminar discontinuity and reduce the in-plane stresses values, which are relevant to buckling phenomena. The First order shear deformation shell models that are usually considered in commercial finite element codes could lead to erroneous conclusions and the use of more computational expensive models that employ solid elements should be introduced. In this contest, the use of refined shell models appears mandatory. Future work should not be limited to simple shell elements (rings and spherical caps) by including complete pressure vessels geometry with FGM layers; effects of both geometrical and physical nonlinearities should be investigated too.

References

[1] S. Chattopadhyay. *Pressure Vessels: Design and Practice*, CRC Press, New York, 2004.

[2] D. Bushnell. *Computerized buckling analysis for shells*, Lockheed Palo Alto Research Laboratory, Palo Alto, 1985.

[3] S.H. Zhang, L. Jiang, B.L. Wang and Z. R. Wang. Finite-element analysis of the integral hydrobulge forming of double-layer gap spherical vessels. *International Journal of Pressure Vessels and Piping*, **68**, 161-167, 1996.

[4] S.H. Zhang, B.L. Wang, Y.L. Shang, X.R. Kong, J.D. Hu, and Z.R. Wang. Three-dimensional finite element simulation of the integral hydrobulge forming of a spherical LPG tank. *International Journal of Pressure Vessels and Piping*, **65**, 47-52, 1996.

[5] M. R. Baum. Rupture of a gas-pressurized cylindrical vessel: the velocity of a detached end-cap. *Journal Loss Pm. Process Ind.*, **8**, 149-161, 1995.

[6] R. Khan and W. Uddin. The stability of conical end caps with spherical tips as end closures form pressure vessels. *International Journal of Pressure Vessels and Piping*, **64**, 11-16, 1995.

[7] A. Tafreshi. Numerical analysis of thin torispherical end closures. *International Journal of Pressure Vessels and Piping*, **71**, 77-88, 1997.

[8] J. Mackerle. Finite elements in the analysis of pressure vessels and piping, an addendum: A bibliography (1996-1998). *International Journal of Pressure Vessels and Piping*, **76**, 461-485, 1999.

[9] J. Mackerle. Finite elements in the analysis of pressure vessels and piping, an addendum: A bibliography (1996-1998). *International Journal of Pressure Vessels and Piping*, **79**, 1-26, 2002.

[10] J. Mackerle. Finite elements in the analysis of pressure vessels and piping, an addendum: A bibliography (20012004). *International Journal of Pressure Vessels and Piping*, **82**, 571-592, 2005.

[11] Z. Li and S.L. Gobbi. Laser welding for lightweight structures. *Journal of Materials Processing Technology*, **70**, 137-144, 1997.

[12] J.G. Teng and X. Lin. Fabrication of small models of large cylinders with extensive welding for buckling experiments. *Thin-Walled Structures*, **43**, 1091-1114, 2005.

[13] D.T. Jones, I.A. Jones and V. Middleton. Improving composite lay-up for non-spherical filament-wound pressure vessels. *Composites: Part A*, **27A**, 311-317, 1996.

[14] D. Cohen. Influence of filament winding parameters on composite vessel quality and strength. *Composites: Part A*, **28A**, 1034-1047, 1997.

[15] D. Cohen, S.C. Mantell and L. Zhao. The effect of fiber volume fraction on filament wound compisite pressure vessel strenght. *Composites: Part B*, **32**, 413-429, 2001.

[16] M. Koizumi, *"The concept of FGM"*, Ceram. Trans. Funct. Graded Mater., 34, 3-10, 1993.

[17] S. Suresh and A. Mortensen, *"Fundamentals of functionally graded materials"*, Barnes and Noble Publications, 1998.

[18] S.Brischetto, R.Leetsch, E.Carrera, T.Wallmersperger and B. Kröplin. Thermo-Mechanical Bending Of Functionally Graded Plates. *Journal of Thermal Stresses*, **31**, 286-308, 2008.

[19] V. Birman, L.W. Bird, Modeling and Analysis of Functionally Graded Materials and Structures. *Applied Mechanics Reviews*, **60**, 195-217, 2007

[20] E. Carrera. Multilayered Shell Theories Accounting for layerwise mixed description - Part I,II. *AIAA Journal*, **37(9)**, 1107-1124, 1999.

[21] E. Carrera. Develompments, ideas and evaluations based upon Reissner's mixed variational theorem in the modeling of multilayered plates and shells. *Applied Mechanics Reviews*, **54(4)**, 301-329, 2001.

[22] Carrera, E. Theories and finite elements for multilayered plates and shells: a unified compact formulation with numerical assessments and benchmarks. *Archivies of Computational Methods in Engineering*, **10**, 215-296, 2003.

[23] J.N. Reddy. *Mechanics of Laminated Composite Plates, Theory and Analysis*. CRC Press, New York, 2004.

[24] E. Carrera, S. Brischetto, A. Robaldo. Variable Kinematic Model for the Analysis of Functionally Graded Material Plates. *AIAA Journal*, **46**, 194-203, 2008.

[25] S. Brischetto and E. Carrera. Importance of Higher Order Modes and Refined Theories in Free Vibration Analysis of Composite Plates. *Journal of Applied Mechanics*, **77**, 2010.

[26] K. Washizu. *Variational methods in elasticity and plasticity*, Pergamon Press, New York, 1968.

[27] E. Reissner. On a certain mixed variational theory and a proposed application. *International Journal for Numerical Methods in Engineering*, **20**, 1366-1368, 1984.

[28] E. Carrera. A class of two dimensional theories for multilayered plates analysis. *Atti Accademia delle Scienze di Torino*. Memorie Scienze Fisiche. **19-20**, 49-87, 1995.

[29] E. Carrera. Multilayered Shell Theories Accounting for layerwise mixed description - Part I,II. *AIAA Journal*. **37(9)**, 1107-1124, 1999.

[30] E. Carrera, An assessment of Mixed and Classical Theories for thermal stress analysis of orthotropic Multilayered Plates. *Journal of Thermal Stress*, **23**, 797-831, 2000.

[31] E. Carrera. Temperature Profile Influence on Layered Plates Response Considering Classical and Advanced Theories,. *AIAA Journal*, **40**, 1885-1896, 2002.

[32] M. Cinefra, S. Brischetto, E. Carrera, Beloueattar S., Thermo-mechanical analysis of functionally graded shells, *Journal of Thermal Stress*, **in press**

[33] E. Carrera, Multilayered Shell Theories Accounting for layerwise mixed description - Part I,II - Governing Equations and Numerical evluations, *AIAA Journal*, **37**, 1107-1124, 1999.

[34] E. Carrera, A study of transverse normal stress effect on vibration of multylayered plates and shells, *Journal of Sound and Vibrations*, **225**(5), 803-829, 1999.

A Explicit form of governing equations of layered shell embedding FGM layers

This section presents the governing equations based on the two used variational statements: Principle of virtual displacement (PVD) and Reissner Mixed Variational Theorem (RMVT). The derivation of governing equation permits to obtain the so-called *fundamental nuclei*. These consist of [3x3] arrays that represent the basic items from which the stiffness matrix of the whole structure can be computed. Detailed derivation procedure is given in the previous works [33], [34].
For a laminate with N_l layers, the PVD for pure mechanical analysis, neglecting any body forces and considering only applied mechanical loads, is formulated as:

$$\sum_{k=1}^{N_l} \int_{\Omega_k} \int_{A_k} \left\{ \delta {\boldsymbol{\epsilon}_{pG}^k}^T \boldsymbol{\sigma}_{pC}^k + \delta {\boldsymbol{\epsilon}_{nG}^k}^T \boldsymbol{\sigma}_{nC}^k \right\} d\Omega_k dz = \sum_{k=1}^{N_L} \delta L_e^k \tag{12}$$

where the integration domains Ω_k and A_k indicate respectively the reference plane of the lamina and its thickness. Subscript G and C indicate geometrical relations and constitutive equations respectively. δL_e^k is the expression of the external work that takes into account of the external loads for a generic layer k.

In the case of shells with constant radii of curvature, the geometrical relations are written in the following matrix form:

$$\boldsymbol{\epsilon}_{pG}^k = [\epsilon_{\alpha\alpha}^k, \epsilon_{\beta\beta}^k, \gamma_{\alpha\beta}^k]^T = (\boldsymbol{D}_p^k + \boldsymbol{A}_p^k)\ \boldsymbol{u}^k\ , \tag{13}$$

$$\boldsymbol{\epsilon}_{nG}^k = [\gamma_{\alpha z}^k, \gamma_{\beta z}^k, \epsilon_{zz}^k]^T = (\boldsymbol{D}_{np}^k + \boldsymbol{D}_{nz}^k - \boldsymbol{A}_n^k)\ \boldsymbol{u}^k\ , \tag{14}$$

where for each layer k the vector of displacement components is $\boldsymbol{u}^k = (u^k, v^k, w^k)$. The explicit form of the introduced arrays follows:

$$\boldsymbol{D}_p^k = \begin{bmatrix} \frac{\partial_\alpha}{H_\alpha^k} & 0 & 0 \\ 0 & \frac{\partial_\beta}{H_\beta^k} & 0 \\ \frac{\partial_\beta}{H_\beta^k} & \frac{\partial_\alpha}{H_\alpha^k} & 0 \end{bmatrix}\ , \quad \boldsymbol{D}_{np}^k = \begin{bmatrix} 0 & 0 & \frac{\partial_\alpha}{H_\alpha^k} \\ 0 & 0 & \frac{\partial_\beta}{H_\beta^k} \\ 0 & 0 & 0 \end{bmatrix}\ , \quad \boldsymbol{D}_{nz}^k = \begin{bmatrix} \partial_z & 0 & 0 \\ 0 & \partial_z & 0 \\ 0 & 0 & \partial_z \end{bmatrix}\ . \tag{15}$$

$$\boldsymbol{A}_p^k = \begin{bmatrix} 0 & 0 & \frac{1}{H_\alpha^k R_\alpha^k} \\ 0 & 0 & \frac{1}{H_\beta^k R_\beta^k} \\ 0 & 0 & 0 \end{bmatrix}\ , \boldsymbol{A}_n^k = \begin{bmatrix} \frac{1}{H_\alpha^k R_\alpha^k} & 0 & 0 \\ 0 & \frac{1}{H_\beta^k R_\beta^k} & 0 \\ 0 & 0 & 0 \end{bmatrix}\ . \tag{16}$$

The coefficients H^k are:

$$H_\alpha^k = A^k\ (1 + \frac{z_k}{R_\alpha^k}), \quad H_\alpha^k = B^k\ (1 + \frac{z_k}{R_\beta^k}), \quad H_z^k = 1$$

where A^k e B^k are the coefficients of first fundamental form of reference surface and them, for shells to have constant curvature, have unit value. ($A^k = B^k = 1$)

Constitutive equations for PVD states:

$$\boldsymbol{\sigma}_{pC}^k = \boldsymbol{Q}_{pp}^k(z)\boldsymbol{\epsilon}_{pG}^k + \boldsymbol{Q}_{pn}^k(z)\boldsymbol{\epsilon}_{nG}^k\ , \tag{17}$$

$$\boldsymbol{\sigma}_{nC}^k = \boldsymbol{Q}_{np}^k(z)\boldsymbol{\epsilon}_{pG}^k + \boldsymbol{Q}_{nn}^k(z)\boldsymbol{\epsilon}_{nG}^k\ . \tag{18}$$

where $Q^k_{pp}, Q^k_{pn}, Q^k_{np}, Q^k_{nn}$ are [3x3] sub-arrays containing the elastic coefficients for an orthotropic layer in the structure reference system.
Similarly, the RMVT (Eq.(7)) for a laminate becomes:

$$\sum_{k=1}^{N_l} \int_{\Omega_k} \int_{A_k} \left\{ \delta \boldsymbol{\epsilon}^T_{pG} \boldsymbol{\sigma}_{pC} + \delta \boldsymbol{\epsilon}^T_{nG} \boldsymbol{\sigma}_{nM} + \delta \boldsymbol{\sigma}^T_{nM} (\boldsymbol{\epsilon}_{nG} - \boldsymbol{\epsilon}_{nC}) \right\} d\Omega_k dz = \sum_{k=1}^{N_L} \delta L^k_e \tag{19}$$

where constitutive equations states:

$$\boldsymbol{\sigma}^k_{pC} = \hat{\boldsymbol{Q}}^k_{pp}(z)\, \boldsymbol{\epsilon}^k_{pG} \;+\; \hat{\boldsymbol{Q}}^k_{pn}(z)\, \boldsymbol{\sigma}^k_{nM} \;, \tag{20}$$

$$\boldsymbol{\epsilon}^k_{nC} = \hat{\boldsymbol{Q}}^k_{np}(z)\, \boldsymbol{\epsilon}^k_{pG} \;+\; \hat{\boldsymbol{Q}}^k_{nn}(z)\, \boldsymbol{\sigma}^k_{nM} \;, \tag{21}$$

where the new coefficients are:

$$\hat{\boldsymbol{Q}}^k_{pp}(z) = \boldsymbol{Q}^k_{pp}(z) - \boldsymbol{Q}^k_{pn}(z) \boldsymbol{Q}^k_{nn}(z)^{-1} \boldsymbol{Q}^k_{np}(z) \;, \qquad \hat{\boldsymbol{Q}}^k_{pn}(z) = \boldsymbol{Q}^k_{pn}(z) \boldsymbol{Q}^k_{nn}(z)^{-1} \;, \tag{22}$$

$$\hat{\boldsymbol{Q}}^k_{np}(z) = -\boldsymbol{Q}^k_{nn}(z)^{-1} \boldsymbol{Q}_{np}(z) \;, \qquad \hat{\boldsymbol{Q}}^k_{nn}(z) = \boldsymbol{Q}^k_{nn}(z)^{-1} \;.$$

In case of FGM layers, the coefficients in Eqs. (17), (22), and (20) vary in the thickness direction z according to a given law:

$$\boldsymbol{Q}(z) = \boldsymbol{Q}_0 * g(z), \tag{23}$$

where $\boldsymbol{Q}_0$ is the reference stiffness matrix and $g(z)$ gives the variation along z. For convenience, the thickness functions given in Eq.(3), are used to approximate $Q(z)$:

$$\boldsymbol{Q}(z) = F_b(z)\boldsymbol{Q}_b + F_t(z)\boldsymbol{Q}_t + F_\gamma(z)\boldsymbol{Q}_\gamma = F_r\, \boldsymbol{Q}_r \quad with\ r = 1, ..., 10 \tag{24}$$

where $\boldsymbol{Q}_r$ are constant in z and *thickness functions* F_r are a combination of Legendre polynomials. Previous formula consists of the unique novelty for the introduction of FGM in the variable kinematic model in the CUF. By considering the approximation given in Eq.(24), it is possible to obtain a general form of constitutive relations for the PVD and RMVT case, they are valid for both cases of functionally graded materials and materials with constant properties through the thickness direction z. For the PVD models, the constitutive equations are:

$$\boldsymbol{\sigma}^k_{pC} = F_r \boldsymbol{Q}^k_{ppr} \boldsymbol{\epsilon}^k_{pG} + F_r \boldsymbol{Q}^k_{pnr} \boldsymbol{\epsilon}^k_{nG} \;, \tag{25}$$

$$\boldsymbol{\sigma}^k_{nC} = F_r \boldsymbol{Q}^k_{npr} \boldsymbol{\epsilon}^k_{pG} + F_r \boldsymbol{Q}^k_{nnr} \boldsymbol{\epsilon}^k_{nG} \;. \tag{26}$$

In the case of RMVT models, the constitutive equations state:

$$\boldsymbol{\sigma}^k_{pC} = F_r \hat{\boldsymbol{Q}}^k_{ppr}\, \boldsymbol{\epsilon}^k_{pG} \;+\; F_r \hat{\boldsymbol{Q}}^k_{pnr}\, \boldsymbol{\sigma}^k_{nM} \;, \tag{27}$$

$$\boldsymbol{\epsilon}^k_{nC} = F_r \hat{\boldsymbol{Q}}^k_{npr}\, \boldsymbol{\epsilon}^k_{pG} \;+\; F_r \hat{\boldsymbol{Q}}^k_{nnr}\, \boldsymbol{\sigma}^k_{nM} \;, \tag{28}$$

where $k = 1, \ldots, N_l$ indicates the considered layers, and $r = 1, \ldots, 10$ is the loop to approximate the FGM properties varying with the z coordinate. In the case of materials with constant properties in z, the loop on r index is not necessary and the material coefficients are constant.

In order to obtain a strong form of differential equations on the domain Ω_k, as well as the correspondence boundary conditions on edge Γ_k, the integration by parts is required. The governing equations on the domain Ω_k, in the PVD case, are:

$$\delta \boldsymbol{u}^{k^T}_s \;: \qquad \boldsymbol{K}^{k\tau sr}_{uu}\, \boldsymbol{u}^k_\tau \;=\; \boldsymbol{P}^k_{us} \tag{29}$$

Boundary conditions of are:

$$\boldsymbol{\Pi}_{uu}^{k\tau sr}\,\boldsymbol{u}_{\tau}^{k} \;=\; \boldsymbol{\Pi}_{uu}^{k\tau sr}\,\bar{\boldsymbol{u}}_{\tau}^{k} \tag{30}$$

In Eq.(29), $\boldsymbol{P}_{u\tau}^{k}$ is the external mechanical load and the fundamental nucleus $\boldsymbol{K}_{uu}^{k\tau sr}$ has to be assembled through the depicted indexes: the internal loop is on index r; τ and s consider the order of expansion in z for the displacements; superscript k indicates the assembling on the number of layers. The fundamental nucleus $\boldsymbol{K}_{uu}^{k\tau sr}$ for the stiffness matrix and the fundamental nucleus $\boldsymbol{\Pi}_{uu}^{k\tau sr}$ for the boundary conditions are:

$$\begin{aligned}\boldsymbol{K}_{uu}^{k\tau sr} = \int_{A_k} \Big[\Big(-\boldsymbol{D}_{p}^{k} + \boldsymbol{A}_{p}^{k}\Big)^{T}\Big(F_r\boldsymbol{Q}_{ppr}^{k}(\boldsymbol{D}_{p}^{k} + \boldsymbol{A}_{p}^{k}) \; + F_r\boldsymbol{Q}_{pnr}^{k}(\boldsymbol{D}_{np}^{k} + \boldsymbol{D}_{nz}^{k} - \boldsymbol{A}_{n}^{k})\Big) + \\ \Big(-\boldsymbol{D}_{np}^{k} + \boldsymbol{D}_{nz}^{k} - \boldsymbol{A}_{n}^{k}\Big)^{T}\Big(F_r\boldsymbol{Q}_{npr}^{k}(\boldsymbol{D}_{p}^{k} + \boldsymbol{A}_{p}^{k}) \; + F_r\boldsymbol{Q}_{nnr}^{k}(\boldsymbol{D}_{np}^{k} + \boldsymbol{D}_{nz}^{k} - \boldsymbol{A}_{n}^{k})\Big)\Big] \\ F_sF_\tau H_\alpha^k H_\beta^k dz \;,\end{aligned} \tag{31}$$

$$\begin{aligned}\boldsymbol{\Pi}_{uu}^{k\tau sr} = \int_{A_k} \Big[\boldsymbol{I}_{p}^{kT}\Big(F_r\boldsymbol{Q}_{ppr}^{k}(\boldsymbol{D}_{p}^{k} + \boldsymbol{A}_{p}^{k}) \; + F_r\boldsymbol{Q}_{pnr}^{k}(\boldsymbol{D}_{np}^{k} + \boldsymbol{D}_{nz}^{k} - \boldsymbol{A}_{n}^{k})\Big) + \\ \boldsymbol{I}_{np}^{kT}\Big(F_r\boldsymbol{Q}_{npr}^{k}(\boldsymbol{D}_{p}^{k} + \boldsymbol{A}_{p}^{k}) \; + F_r\boldsymbol{Q}_{nnr}^{k}(\boldsymbol{D}_{np}^{k} + \boldsymbol{D}_{nz}^{k} - \boldsymbol{A}_{n}^{k})\Big)\Big] F_sF_\tau H_\alpha^k H_\beta^k dz \;.\end{aligned} \tag{32}$$

$\boldsymbol{I}_{p}^{k}$ and $\boldsymbol{I}_{np}^{k}$ are identity matrices to perform the integration by parts.

$$\boldsymbol{I} = \begin{bmatrix}1 & 0 & 0\\ 0 & 1 & 0\\ 0 & 0 & 1\end{bmatrix} \;, \quad \boldsymbol{I}_{p}^{k} = \begin{bmatrix}\frac{1}{H_\alpha^k} & 0 & 0\\ 0 & \frac{1}{H_\beta^k} & 0\\ \frac{1}{H_\beta^k} & \frac{1}{H_\alpha^k} & 0\end{bmatrix} \;, \quad \boldsymbol{I}_{np}^{k} = \begin{bmatrix}0 & 0 & \frac{1}{H_\alpha^k}\\ 0 & 0 & \frac{1}{H_\beta^k}\\ 0 & 0 & 0\end{bmatrix} \;. \tag{33}$$

The governing equations in the RMVT case are:

$$\delta\boldsymbol{u}_{s}^{k} : \boldsymbol{K}_{uu}^{k\tau sr}\boldsymbol{u}_{\tau}^{k} + \boldsymbol{K}_{u\sigma}^{k\tau sr}\boldsymbol{\sigma}_{n\tau}^{k} = \boldsymbol{P}_{us}^{k}\delta\boldsymbol{\sigma}_{ns}^{k} : \boldsymbol{K}_{\sigma u}^{k\tau sr}\boldsymbol{u}_{\tau}^{k} + \boldsymbol{K}_{\sigma\sigma}^{k\tau sr}\boldsymbol{\sigma}_{n\tau}^{k} = 0$$

four fundamental nuclei relative to stiffness array are obtained. These are completely different from those obtained in the PVD case while the inertial array does not change.
Corresponding boundary conditions of Neumann type are:

$$\boldsymbol{\Pi}_{uu}^{k\tau sr}\boldsymbol{u}_{\tau}^{k} + \boldsymbol{\Pi}_{u\sigma}^{k\tau sr}\boldsymbol{\sigma}_{n\tau}^{k} = \boldsymbol{\Pi}_{uu}^{k\tau sr}\bar{\boldsymbol{u}}_{\tau}^{k} + \boldsymbol{\Pi}_{u\sigma}^{k\tau sr}\bar{\boldsymbol{\sigma}}_{n\tau}^{k}$$

The fundamental nuclei can be obtained:

$$\boldsymbol{K}_{uu}^{k\tau sr} = \int_{A_k} \Big[(-\boldsymbol{D}_{p}^{k} + \boldsymbol{A}_{p}^{k})^{T}(F_r\hat{\boldsymbol{Q}}_{ppr}^{k}(\boldsymbol{D}_{p}^{k} + \boldsymbol{A}_{p}^{k}))\Big] F_sF_\tau H_\alpha^k H_\beta^k dz \;, \tag{34}$$

$$\boldsymbol{K}_{u\sigma}^{k\tau sr} = \int_{A_k} \Big[(-\boldsymbol{D}_{p}^{k} + \boldsymbol{A}_{p}^{k})^{T}(F_r\hat{\boldsymbol{Q}}_{pnr}^{k}) + (-\boldsymbol{D}_{np}^{k} + \boldsymbol{D}_{nz}^{k} - \boldsymbol{A}_{n}^{k})^{T}\Big] F_sF_\tau H_\alpha^k H_\beta^k dz \;, \tag{35}$$

$$\boldsymbol{K}_{\sigma u}^{k\tau sr} = \int_{A_k} \Big[(\boldsymbol{D}_{np}^{k} + \boldsymbol{D}_{nz}^{k} - \boldsymbol{A}_{n}^{k}) - (F_r\hat{\boldsymbol{Q}}_{npr}^{k})(\boldsymbol{D}_{p}^{k} + \boldsymbol{A}_{p}^{k})\Big] F_sF_\tau H_\alpha^k H_\beta^k dz \;, \tag{36}$$

$$\boldsymbol{K}_{\sigma\sigma}^{k\tau sr} = \int_{A_k} \Big[-F_r\hat{\boldsymbol{Q}}_{nnr}^{k}\Big] F_sF_\tau H_\alpha^k H_\beta^k dz \;, \tag{37}$$

The nuclei for boundary conditions on edge Γ_k are:

$$\mathbf{\Pi}_{uu}^{k\tau sr} = \int\limits_{A_k} \left[\boldsymbol{I}_p^{k\,T} F_r \hat{\boldsymbol{Q}}_{ppr}^k (\boldsymbol{D}_p^k + \boldsymbol{A}_p^k) \right] F_s F_\tau H_\alpha^k H_\beta^k dz \ , \tag{38}$$

$$\mathbf{\Pi}_{u\sigma}^{k\tau sr} = \int\limits_{A_k} \left[\boldsymbol{I}_p^{k\,T} F_r \hat{\boldsymbol{Q}}_{pnr}^k + \boldsymbol{I}_{np}^{k\ T} \right] F_s F_\tau H_\alpha^k H_\beta^k dz \ . \tag{39}$$

$Material$	$E[Gpa]$	$\rho[Kg/m^3]$	$\sigma_f[Mpa]$	ν
$Titanium$	105	4507	240	0.3
$Aluminium$	70	2700	124	0.3
$Steel$	220	7850	580	0.3
$CarbonFiber$	230	1800	3600	0.3
FGM	$Var.$	$Var.$	$-$	0.3

Table 1: Material properties.

		Ti	Al	St	C
W	[Kg]	1274.32	764.1	2221.55	509.4
$\sigma_{Eq_{MAX}}$	[MPa]	25.72	25.72	25.72	25.72
σ_f	[MPa]	240	124	580	3600
p_{Max}	[MPa]	18.66	9.64	45.10	279.92

Table 2: Comparison of pressure vessels made by single layer wall of constant thickness.

		Ti/C	Ti/FGM/C	Ti/FGM*/C
h_Tot	[m]	0.1	0.1	1.2
h_{FGM}	[m]	$-$	0.02	0.02
h_C	[m]	0.09	0.07	0.9

Table 3: Thickness data of the considered pressure vessels walls.

		Ti/C	Ti/FGM/C	Ti/FGM*/C
$Weight$	[Kg]	577.82	577.82	693.12
$\sigma_{Eq_{MAX}}$	[MPa]	13.627	14.377	11.610
τ_{MAX}	[MPa]	0.4831	0.4703	0.5193
$\tau_{i.l.(1)}$	[MPa]	–	0.3409	0.3276
$\tau_{i.l.(2)}$	[MPa]	0.1001	0.1117	0.1019

Table 4: Comparison of weight and allowable stresses.

$Max\ value$	Ti/C	Ti/FGM/C	advantage	
$\tau_{\alpha\beta}$	[MPa]	8.8081	7.9503	$*$
$\sigma_{\beta\beta}$	[MPa]	12.809	13.280	
$\tau_{\alpha z}$	[MPa]	0.4831	0.4703	$*$
$\tau_{\beta z}$	[MPa]	0.8762	0.8548	$*$
	Maximum pressure obtained by various criteria			
$p(\tau)$	[MPa]	1791.0	1845.0	$*$
$p(\sigma_{Eq})$	[MPa]	264.18	250.40	

Table 5: Cylindrical shell under static pressure. Comparison between pure two-layered wall and two-layered wall with FGM layers.

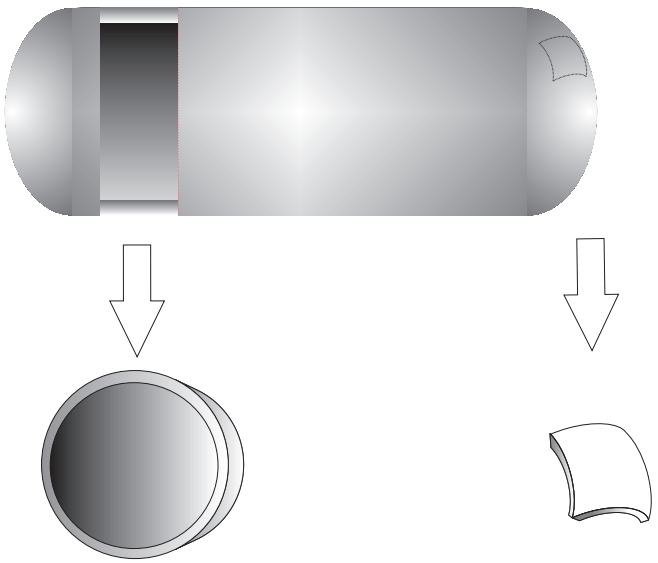

Figure 1: Geometry of pressure vessel. Cylindrical and spherical shells analyzed in the present work.

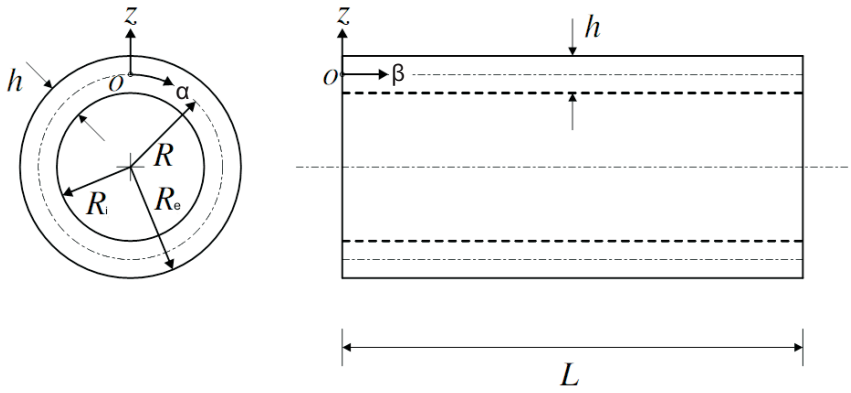

Figure 2: Geometry of cylindrical shell.

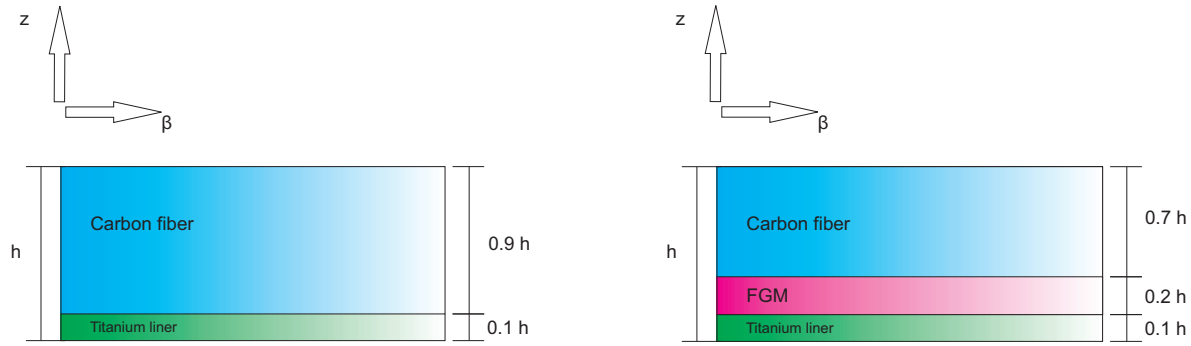

Figure 3: Layers and wall lay-up geometry of the considered shells.

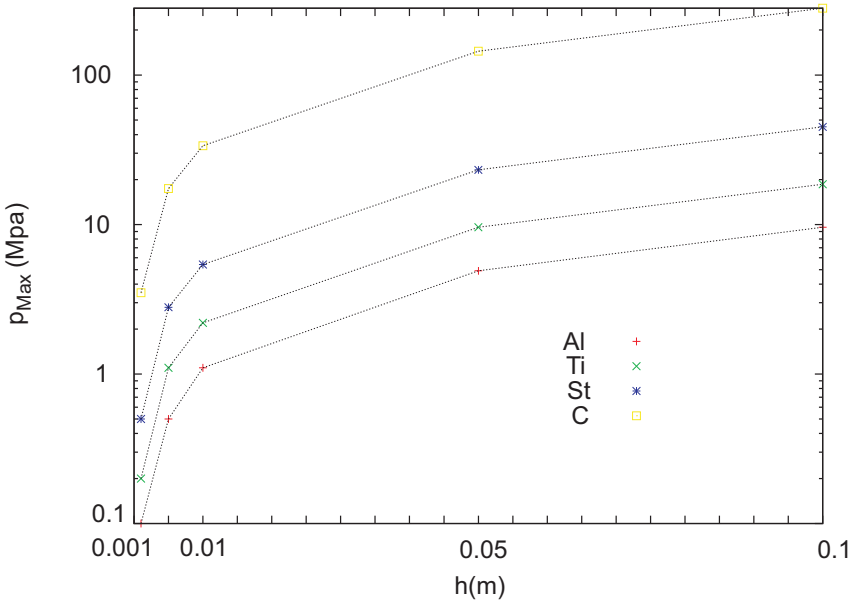

Figure 4: Allowable pressure vs wall thickness. Comparison of various wall lay-up for a cylindrical shell.

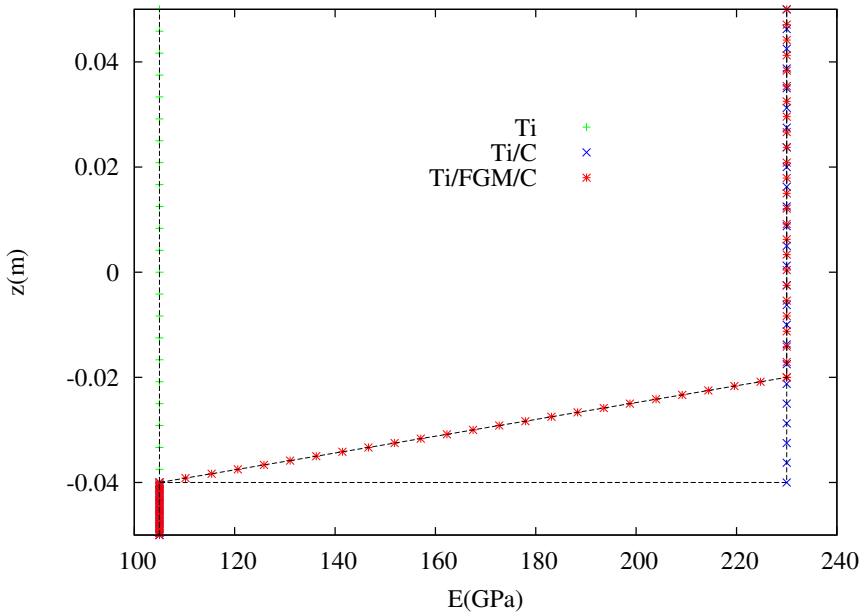

Figure 5: Variation of elastic modulus through the thickness for the considered wall lay-up.

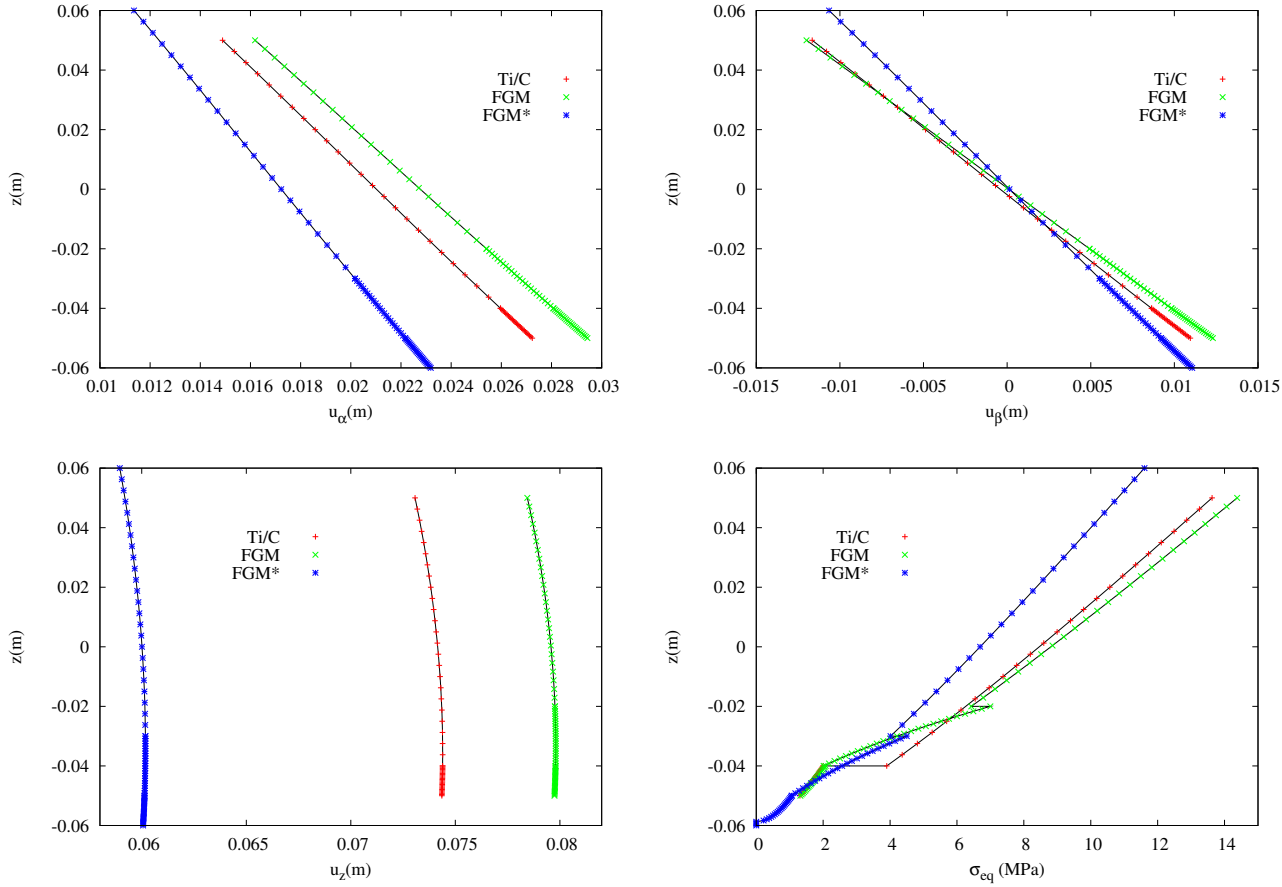

Figure 6: Cylindrical shell under mechanical loading. Comparison of the through-the-thickness distribution of displacement variables.

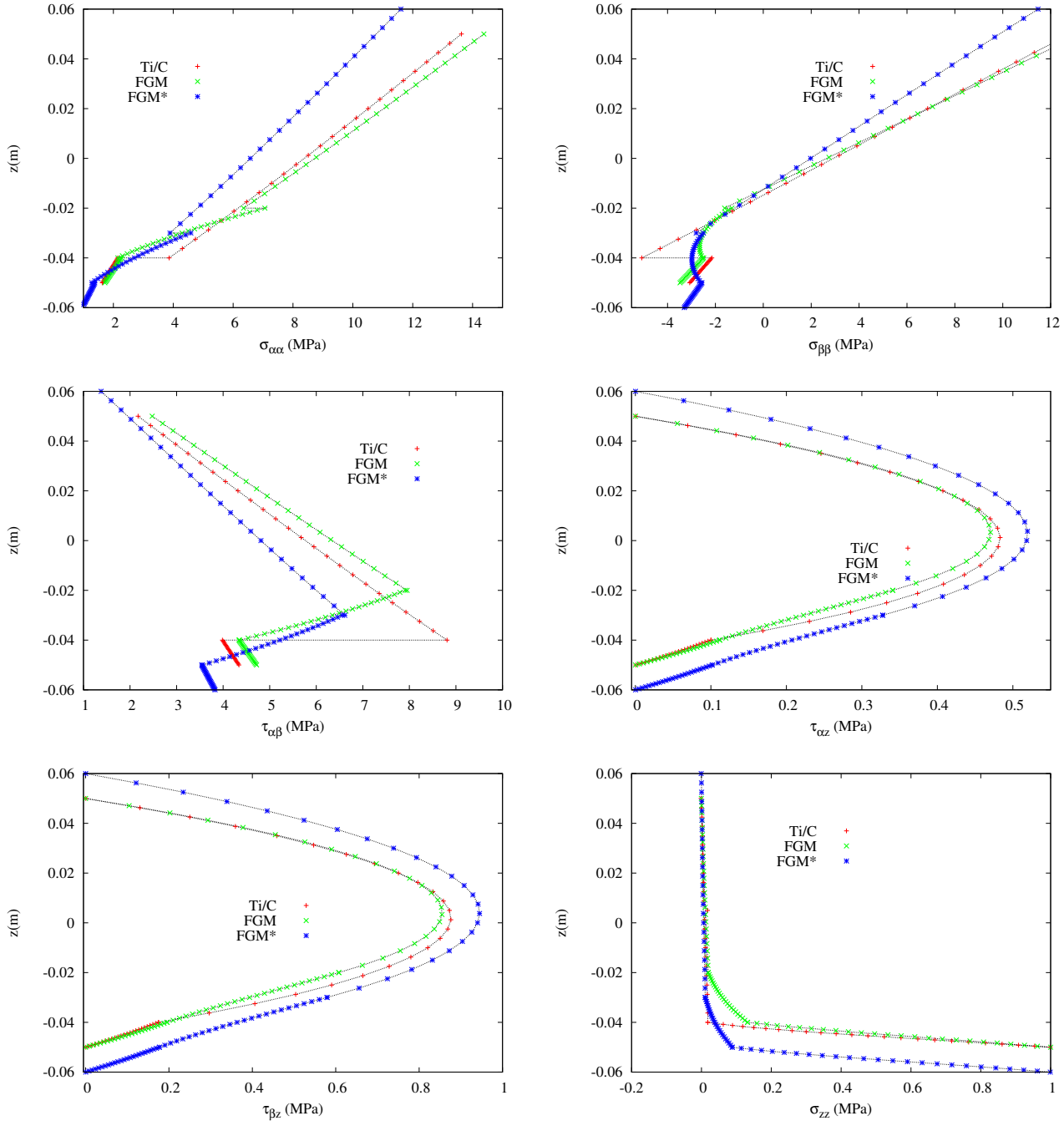

Figure 7: Cylindrical shell. Comparison of stress fields.

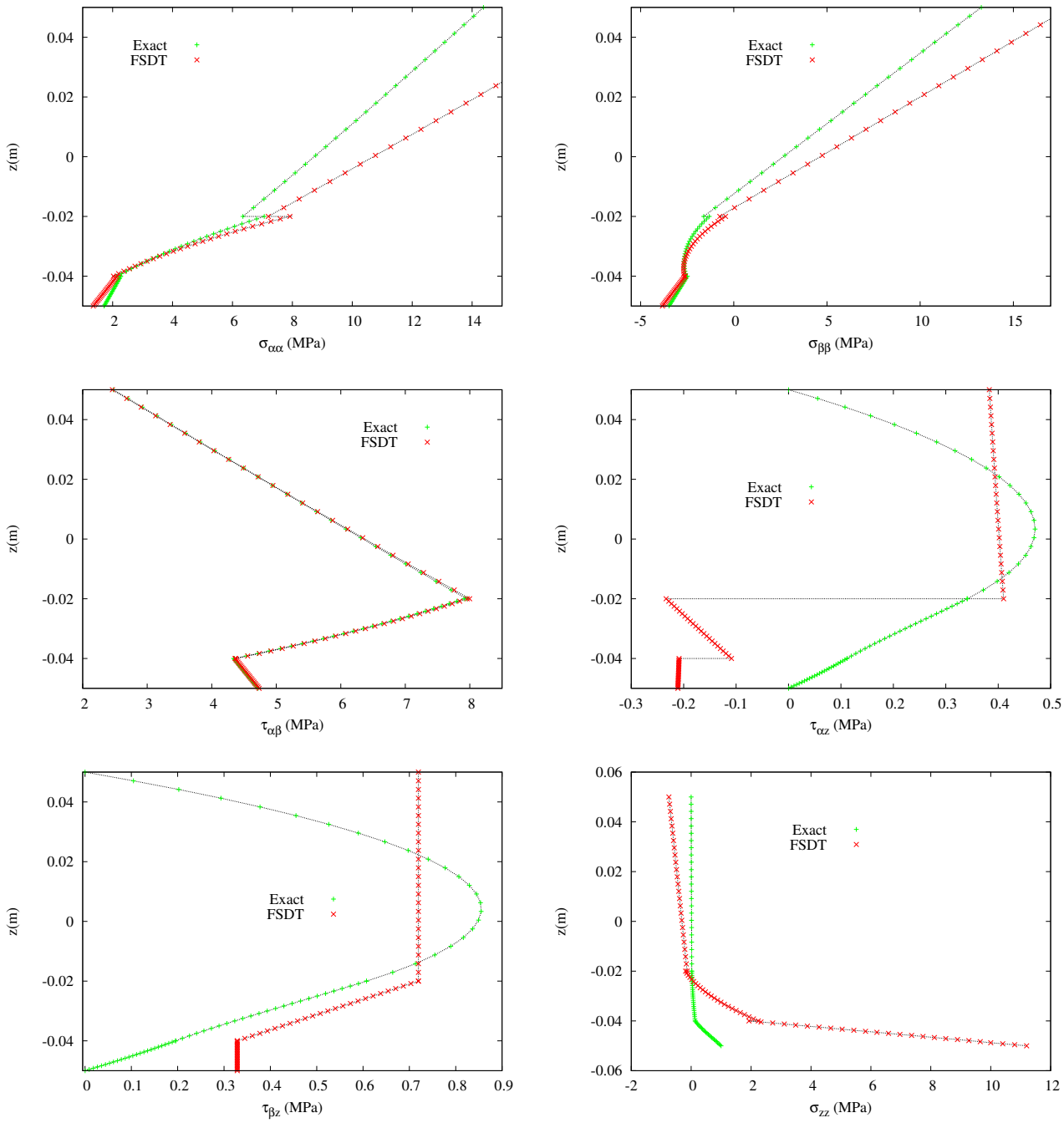

Figure 8: Cylindrical shell under mechanical loading. Comparison between quasi-3D solution and FSDT type analysis.

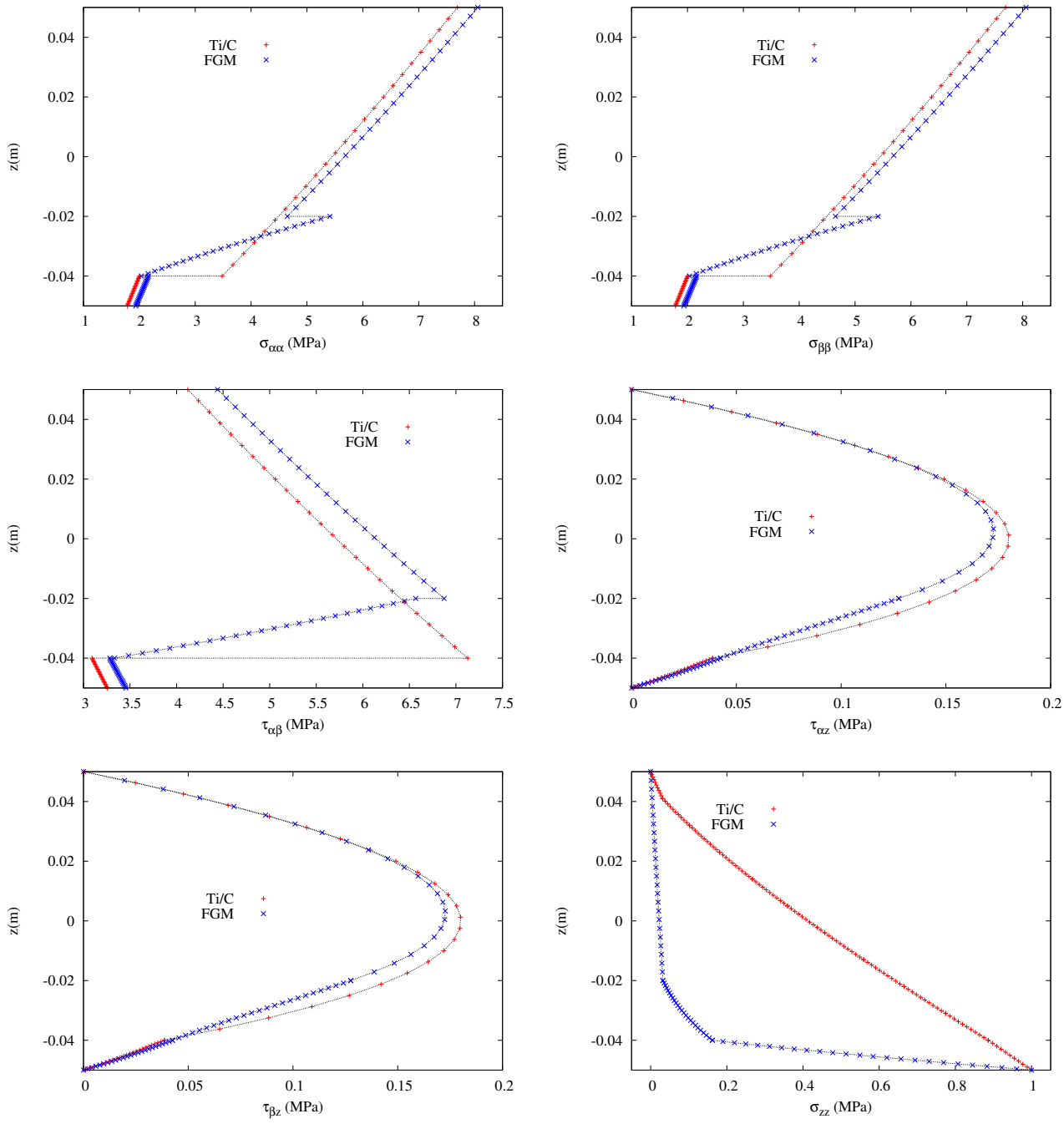

Figure 9: Spherical panel. Comparison of stress fields.

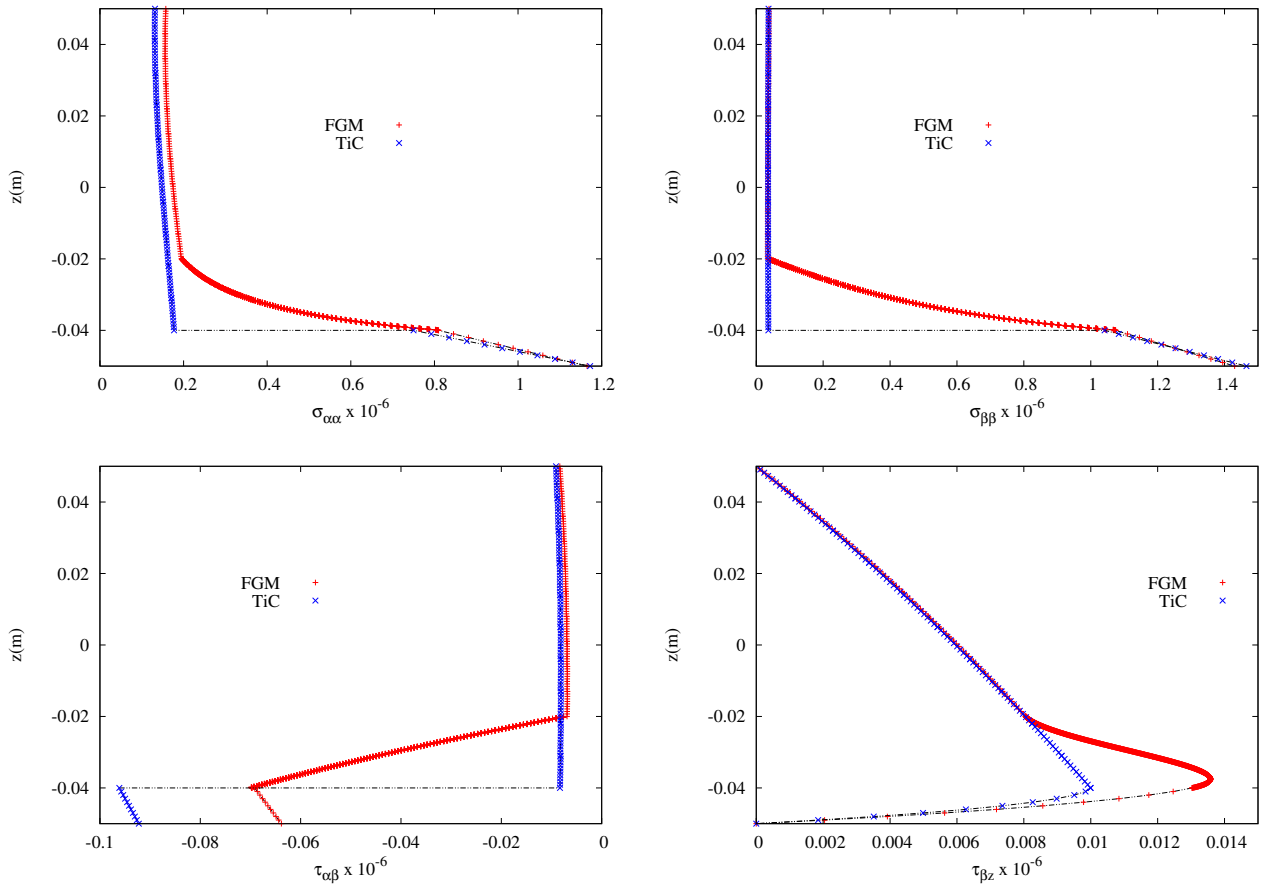

Figure 10: Cylindrical shell under thermal loading. Comparison of stress fields.